Journal of Medical Entomology, 56(6), 2019, 1636–1649
doi: 10.1093/jme/tjz114
Advance Access Publication Date: 19 July 2019
Research

Microanatomy of the American Malaria Vector *Anopheles aquasalis* (Diptera: Culicidae: Anophelinae) Midgut: Ultrastructural and Histochemical Observations

Djane C. Baia-da-Silva,[1,2,6] Alessandra S. Orfanó,[3] Rafael Nacif-Pimenta,[3] Fabricio F. de Melo,[4] Maria G. V. B. Guerra,[1,2] Marcus V. G. Lacerda,[1,2,5] Wuelton M. Monteiro,[1,2] Paulo F. P. Pimenta[1,2,3]

[1]Fundação de Medicina Tropical Dr. Heitor Vieira Dourado, Av. Pedro Teixeira, 25, Dom Pedro, Manaus CEP 69040-000, Manaus, AM, Brazil, [2]Programa de Pós-Graduação em Medicina Tropical, Universidade do Estado do Amazonas, Av. Pedro Teixeira, 25, Dom Pedro, Manaus CEP 69040-000, Manaus, AM, Brazil, [3]Instituto Leônidas and Maria Deane, Fundação Oswaldo Cruz-Manaus, Rua Terezina, 476, Adrianópolis, CEP 69057-070, Manaus, AM, Brazil, [4]Instituto Multidisciplinar em Saúde, Universidade Federal da Bahia, Rua Hormindo Barros, 58, Candeias, CEP 45029-094, Vitória da Conquista, BA, Brazil, [5]Instituto de Pesquisas René Rachou, Fundação Oswaldo Cruz-Minas Gerais, Av. Augusto de Lima, 1715, Barro Preto, CEP 30190002, Belo Horizonte, MG, Brazil, and [6]Corresponding author, e-mail: djane.claryss@gmail.com

Subject Editor: Julian Hillyer

Received 23 November 2018; Editorial decision 14 June 2019

Abstract

The mosquito gut is divided into foregut, midgut, and hindgut. The midgut functions in storage and digestion of the bloodmeal. This study used light, scanning (SEM), and transmission (TEM) electron microscopy to analyze in detail the microanatomy and morphology of the midgut of nonblood-fed *Anopheles aquasalis* females. The midgut epithelium is a monolayer of columnar epithelial cells that is composed of two populations: microvillar epithelial cells and basal cells. The microvillar epithelial cells can be further subdivided into light and dark cells, based on their affinities to toluidine blue and their electron density. FITC-labeling of the anterior midgut and posterior midgut with lectins resulted in different fluorescence intensities, indicating differences in carbohydrate residues. SEM revealed a complex muscle network composed of circular and longitudinal fibers that surround the entire midgut. In summary, the use of a diverse set of morphological methods revealed the general microanatomy of the midgut and associated tissues of *An. aquasalis*, which is a major vector of *Plasmodium* spp. (Haemosporida: Plasmodiidae) in America.

Key words: *Anopheles aquasalis*, midgut, fluorescent lectin labeling, ultrastructure

Malaria is a febrile, infectious disease caused by protozoan parasites of the genus *Plasmodium*, considered a significant public health problem worldwide. It is estimated that in 2017, 219 million cases occurred worldwide, which resulted in 435,000 deaths. Although the incidence rates of malaria declined globally between 2010 and 2017, 72–59 cases per 1,000 population are at risk (WHO 2018). *Plasmodium* species are transmitted to humans through the bite of the female *Anopheles* mosquitoes. The *Anopheles* genus is made up of about 430 species, but only around 70 species are considered malaria vectors (Hay et al. 2010, Sinka et al. 2012).

The mosquito *Anopheles aquasalis* is a critical American malaria vector that breeds in brackish coastal marshes and is predominant along the Atlantic Coast, including Venezuela, where it is considered to be a primary vector of *Plasmodium vivax* (Haemosporida: Plasmodiidae) in the Amazonian coast (Deane 1986, Laubach et al. 2001). This species has been colonized for several years and used as the leading model for interaction studies of American *Anopheles* vector with the malaria-causing *Plasmodium* parasite (review in Pimenta et al. 2015). This mosquito is easily maintained in the laboratory. Some studies have contributed to knowledge of its biology (Perez and Conn 1992; Conn et al. 1993; Flores-Mendoza et al. 1996; Maldonado et al. 1997; Fairley et al. 2002, 2005; Da Silva 2006) and its susceptibility to *Plasmodium* infections (Bahia et al. 2010, 2011, 2013; Rios-Velásquez et al. 2013; Pimenta et al. 2015; Orfanó et al. 2016a,b; Pinilla et al. 2018; Martins-Campos et al. 2018; Baia-da-Silva et al. 2019). However, there are no morphological and structural studies of the midgut of this mosquito vector, which is surprising because the midgut is the first target of *Plasmodium*.

The midgut in hematophagous insects is the primary organ responsible for blood digestion and absorption, nutrient absorption, ion

exchange, synthesis, and release of neurohormones. Morphological aspects of the midgut organization have been described for mosquitoes at different stages of life or under different feeding conditions (Bertram and Bird 1961, Bauer et al. 1977, Hecker 1977, Houk 1977, Houk and Hardy 1982, Okuda et al. 2005). The mosquito midgut is divided into anterior (AMG) and posterior (PMG) midgut regions with distinct physiological functions (Richards 1975, Billingsley and Lehane 1996). The AMG leads digestion and absorption of sugar content from food, whereas the PMG promotes the synthesis of the peritrophic matrix (PM) and digestive enzymes, storage of the ingested bloodmeal and transport, absorption of blood-digesting metabolites. The midgut is a simple organ consisting of a single columnar epithelium resting on a basal lamina, which is externally surrounded by a complex muscle network of well-organized circular and longitudinal fibers. The main epithelial cells can be classified accordingly to their functions into digestive cells, regenerative cells, and endocrine cells (Brown et al. 1986, Billingsley 1990, Billingsley and Lehane 1996, Chapman 1998, Onken and Moffett 2015).

A comprehensive understanding of the mosquito vector midgut should provide fundamental information about parasite–vector interactions, which could be used in intervention strategies aiming at disrupting the parasite life cycle (e.g., as transmission-blocking vaccines). Moreover, the midgut cells are integral to bloodmeal digestion and the interaction with occasional ingested parasites, including *Plasmodium* sp. (Vega-Rodriguez et al. 2014, Pimenta et al. 2015, Bennink et al. 2016).

Here, we study for the first time the structure of the midgut of *An. aquasalis*, a prominent New World malaria. By examining the nonblood-fed midgut of females, we show that a filamentous network covers the entire midgut epithelium, which is similar only to *Aedes aegypti* L. (Diptera: Culicidae) (Zieler et al. 2000). Also, as seen in *Ae. aegypti* (Shahabuddin and Pimenta 1998), the *An. aquasalis* midgut has predominantly two main types of microvillar columnar epithelial cells and scarcely distributed small basal cells. We also show the presence of carbohydrate residues, as detected by FITC-labeled lectins. These findings have not been described before in other *Anopheles* mosquitoes.

Materials and Methods

Mosquito Rearing

Anopheles aquasalis were reared at 27°C and 80% humidity on a 12-h light/dark cycle as described elsewhere (Baia-da-Silva et al. 2018). Briefly, the larvae were reared in unchlorinated water containing table salt at a final concentration of 2 g/liter. They were fed with commercial fish food Tetramin Tropical Flakes. Adult mosquitoes were fed ad libitum with 10% sucrose solution.

Midgut Dissection and Fixation

Fifty midguts of 3- to 5-d-old nonblood fed (fed on sugar only) *An. aquasalis* females were carefully dissected in phosphate-buffered saline (PBS) pH 7.4 under a stereoscope. Midguts were fixed at room temperature (RT) for 24 h with 2.5% glutaraldehyde (Ted Pella, Altadena, CA) in 0.1 M cacodylate buffer (Sigma Aldrich, St. Louis, MO) for histology and electron microscopy (Pimenta and de Souza 1983). Some midgut samples were instead fixed with a 4% formaldehyde solution in PBS at 4°C for 3 h and used confocal microscopy. Samples were washed and stored in PBS at 4°C before processing for histology and electron and confocal laser microscopy (CLM) procedures. For ruthenium red (RR; Sigma Aldrich) labeling, the midguts were fixed for 12 h with the same glutaraldehyde solution plus 0.5 mg/ml RR at RT.

Histology

The fixed midguts were dehydrated and embedded with Historesin (Leica Nussloch, Germany) according to the manufacturer's instructions. Histological 2-µm sections were obtained, then stained with 1% toluidine blue (TB; Sigma Aldrich) solution for 3 min, washed, and mounted on glass slides to be analyzed and photographed under an optical microscope (Pimenta et al. 1994, Secundino et al. 2005).

Scanning and Transmission Electron Microscopy

The glutaraldehyde-fixed midguts were post-fixed with 1% osmium tetroxide (Sigma Aldrich) in 0.1 M cacodylate buffer containing 0.8% potassium ferricyanide (Sigma Aldrich) for 30 mim. For transmission electron microscopy (TEM), the midguts were dehydrated in ascending concentration of acetone and embedded in Epon resin (Ted Pella) as described by the manufacturer. Ultrathin sections were cut using an ultramicrotome and stained with uranyl acetate (Sigma Aldrich) and lead citrate (Sigma Aldric) for observation and analysis. For scanning electron microscopy (SEM), some post-fixed entire guts or guts that has been fractured with an entomological pin were washed in buffer solution, dehydrated using a grades acetone series, and dried with a critical point apparatus (Emitech K850, USA). Samples were covered with a layer of 20 nm of gold particles and observed under SEM (Pimenta and de Souza 1983, Secundino et al. 2005).

Cytochemistry Labeling with RR

The fixed midguts for RR cytochemistry were post-fixed with 1% OsO_4 plus 0.5 mg/ml RR for 2 h at RT (Dierichs 1979) washed several times in PBS buffer and processed for TEM as described above. The ultra-fine sections were observed without postcontrastation.

Confocal Laser Microscopy

The formaldehyde-fixed midguts were washed with PBS and incubated in 1% bovine albumin solution (PBS/BSA) for 30 min. Samples were incubated in a dark room with different commercial FITC-labeled lectins (1:1,000 PBS/BSA; Sigma Aldrich) for 1 h and/or with GFP-Phalloidin (1:1,000 PBS/BSA; actin marker; Sigma Aldrich) or Topro-3-iodide (nuclear marker; ThermoFisher, Waltham, MA) for 24 h. The lectins and their sugar-binding-specific residues used were: PNA (*Arachis hypogaea*) = Galβ1 3GalNAcα1-Ser/Thr; LPL (*Limulus polyphemus*) = N-acetyl-D-galactosamine, N-acetyl-α-D-galactosamine acid N-acetyl-neurominic; WGA (*Triticum vulgaris*) = GlcNAcβ1-4GlcNAcβ1-4GlcNAc, Neu5Ac (sialic acid); CONA (*Conavalia ensiformis*) = α-D-mannosyl α-D-glucosyl residues; WFA (*Wisteria floribunda*) = galNaC; UEA (*Ulex europaeus*) = Fucα1-2Gal-R; BS1 (*Bandeiraea simplicifolia*) = α-D-galactosyl and N-acetyl-α-D-glalactosminyl; and RCA (*Ricinus eommunis*) = GalNAc and B-D-gal (Table 1). Under confocal microscopy, FITC excitation and emission wavelengths are approximately 495 nm/521 nm, while the GFP wavelength is 36–395 nm. The labeled samples were mounted on glass slides with antifading Mowiol solution (Menghi et al. 1997).

Results

General Topography of the Nonblood Fed *An. aquasalis* Gut

The *An. aquasalis* gut can be divided into foregut, midgut, and hindgut (Figs. 1A and 2A). The foregut is thin and irregular (Fig. 1A [insert]

Table 1. Labeling patterns of the thoracic and abdominal midguts by FITC-labeled lectins

Cell structure/lectin	PNA	LPL	WGA	CONA	WFA	UEA	BS1	RCA
Cytoplasmic vesicles	–	+	–	++	+	+	+++	++
Microvilli	+++	–	–	+++	–	–	–	+++
Basal-lateral nembranes	–	+	+++	+	+	+	–	+
Muscle fibers	–	–	–	–	–	–	++	–
Tracheola	–	–	–	–	–	+	+	–

PNA (*Arachis hypogaea*) = Galβ1-3GalNAcα1-Ser/Thr; LPL (*Limulus polyphemus*) = N-acetyl-D-galactosamine, N-acetyl-α-D-galactosamine acido N-acetyl-neurominico; WGA (*Triticum vulgaris*) = GlcNAcβ1-4GlcNAcβ1-4GlcNAc, Neu5Ac (sialic acid); CONA (*Conavalia ensiformis*) = α-D-mannosyl α-D-glucosyl residues; WFA (*Wisteria floribunda*) = galNaC; UEA (*Ulex europaeus*) = Fucα1-2Gal-R; BS1 (*Bandeiraea simplicifolia*) = α-D-galactosyl and N-acetyl-α-D-glalactosminyl; RCA (*Ricinus eommunis*) = GalNAc and B-D-galactosamine; LENTIL (*Lens culinaris*) = fucosylated core region of bi- and triantennary complex type and N-glycans.

Fluorescent FITC lectins are shown as negative labeling (–) or through labeling intensity (+ to ++).

and B). The esophageal diverticulum attaches to the foregut through a canaliculus and presents a smooth surface (Fig. 2B [left insert]). The foregut is connected to the midgut through the stomodeal valve (cardiac valve; Figs. 1A (insert), B, and 2A and B). The stomodeal valve is delimited by a single layer of cubic cells with a muscular structure inside and little affinity for the TB staining (Fig.1B). Externally the stomodeal valve presents circular and longitudinal muscle fibers of smooth delimitation appearing to be highly stretched (Fig. 2C). Tracheas were also seen on the external surface of the entire organ (Fig. 2C). Tracheas bifurcate to form smaller caliber tracheoles (Fig. 2C). The stomodeal valve contains six muscular protrusions of different sizes (as shown by SEM of fractured midguts) and its muscle fibers migrate toward the intestinal lumen (Fig. 2D).

The midgut is a tubular-shaped structure and can be divided into two distinct regions: AMG and PMG. The AMG starts at the stomodeal/valve and extends to the first two abdominal segments of the mosquito body. The PMG is easily distinguished from the AMG because it is more dilated and has a sac-shaped corrugated feature that spreads toward the pyloric triangle, where the Malpighian tubules are inserted (Figs. 1A and 2A). The hindgut is continuous with the PMG (Figs. 1A and 2A) but separated by a prominent structure: the pyloric valve (Fig. 1H). Externally, the hindgut has several subunits of circular constraints that are uniformly distributed in its external surface (Fig. 2J).

Structural Characteristics of the Nonblood Fed *An. aquasalis* Midgut and the Epithelial Cell Populations

The histological sections stained with TB provide details of the midgut epithelium and the presence of similar epithelial cell populations within both the AMG and the PMG. The AMG has a columnar epithelium that is composed of bulky epithelial cells with large rounded-central nuclei (Fig. 1C and D). The PMG has a pseudostratified epithelium but with epithelial cells with main internal cellular structures similar to the AMG (Fig. 1E–G). The apical microvillar surfaces of the main epithelial cells (Fig. 2E and F) are full of delicate, straight microvilli that in some areas have attached bacteria (Fig. 2F and H), which are associated with a uniform filamentous network (Fig. 2F). These filaments are thinner than the microvilli and form covering the entire midgut surface (Fig. 2G).

The epithelial cell cytoplasm of the two regions has homogeneously dispersed basophilic granular material and small cytoplasmic vacuoles (Fig. 1C–G). The TB stain also revealed that the epithelium surface is covered by a noticeable brush border with a metachromatic affinity (Fig. 1D–F). Furthermore, these histological sections also showed that the midgut has two main epithelial cell populations with different staining affinities: the dark cells (high-affinity staining) and the light cells (moderate-affinity staining; Fig. 1C, F, and G).

TEM confirmed the presence of these two distinct cell populations, showing ultrastructural difference such as distinct electron densities and different concentration and types of organelles (Fig. 3A–E). The light cells have few organelles, contain some dense granules and vesicles with different sizes and densities that are scarcely distributed in the cytoplasm, and the endoplasmic reticulum is dispersed in a linear and spiral form (Figs. 3A and 4C). In contrast, the dark cells have more mitochondria, a densely distributed endoplasmic reticulum, and several vesicles with distinct electron densities at different locations within the cytoplasm (Figs. 3C and 4B and D). The ultrastructure of both epithelial cells shows long slim microvilli on their surface (Figs. 3A, C, and D, and 4A, B, and D) and confirmed the presence of some attached bacteria (Fig. 4A). Also, TEM revealed that cells junctions are present between the epithelial cells, including a unique junctional complex located close to the apical region of the midgut epithelium (Fig. 4C and D).

With the use of RR labeling associated with TEM, the dark cells display a high electron-dense cytoplasm with a marked distribution of endoplasmic reticulum cisterns, whereas light cells have an electron-lucent cytoplasm (Fig. 3B and D). Also, in the dark cells, the RR shows strong linear and discontinuous reactions on the microvillar surface of the two midgut regions (Fig. 3D [insert]). In addition, the RR labeling highlights the appearance of dense amorphous structures in the basal lamina and basal labyrinth of the entire midgut epithelium, as well as in the muscle fibers that surround the midgut (Figs. 3B and D, and 4F and G). Within the basal portion of the PMG, the epithelial cells are supported by a convoluted basal lamina that forms the basal labyrinth with mitochondria (Fig. 3A and D). In the PMG, the basal lamina is thick, wrinkled, dense, and slightly striated and is composed of several thick layers (Fig. 4G).

Histology and TEM also showed the presence of small dense basal cells distributed in the midgut epithelium (Figs. 1D and F, and 4E). These basal cells are always in contact with the basal lamina and their cytoplasm is poor in organelles. These basal cells have large voluminous nuclei compared to their cell size, with condensed chromatin and a nucleolus (Fig. 4E).

The Muscle Network and the Cytoskeleton of the Nonblood Fed *An. aquasalis* Midgut

SEM and CLM revealed numerous characteristics of the midgut muscle network and its cytoskeleton. The entire midgut is completely covered by a complex muscle network composed of longitudinal and circular fibers (Fig. 5A–E). The longitudinal muscle fibers are separated from each other by irregular spaces and superimposed on the circular muscle fibers (Fig. 5A–E). The muscle network is a continuous structure linking the two midgut regions (Fig. 5C) but

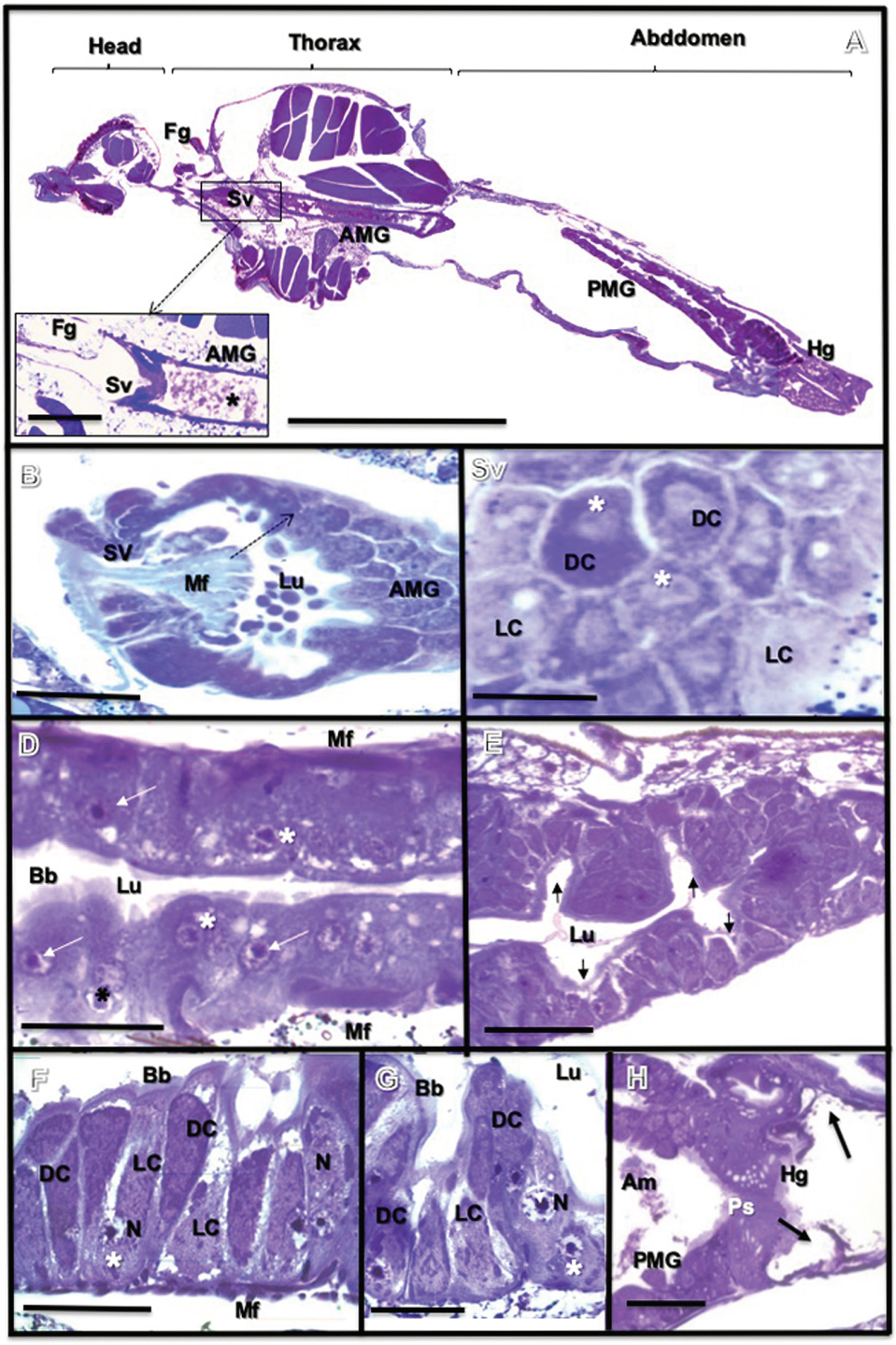

Fig. 1. Histology of the nonblood fed *Anopheles aquasalis*. (A) View of entire mosquito. The composed images of longitudinal histological sections showing head, thorax, and abdomen. Topographical divisions are seen in foregut (Fg), anterior midgut (AMG), posterior midgut (PMG), and hindgut (Hg). The inset shows the stomodeal valve (Sv) (arrow) separating the Foregut from the AMG. An asterisk indicates the presence of metachromatic material and bacteria in the lumen. Bar: 100 μm. (B) Stomodeal valve. Large view of the stomodeal valve (Sv) delimited by a single layer of cubic cells (arrow). Muscle fibers (Mf) migrate toward the gut lumen (Lu). AMG = anterior midgut. Bar: 10 μm. (C) and (D) Anterior midgut. Epithelium with light (LC) and dark (DC) epithelial cells (C). A transversal section showing a single columnar epithelium constituted of bulky cells with an apparent nucleus (asterisks) and evident nucleolus (arrows) (D). Lu = lumen, Bb = brush border, Mf = muscle fibers. Bars: 5 μm (C) and 10 μm (D). (E)–(H) Posterior midgut. Typical folding epithelium (arrows) with fund sacs (E). The simple pseudostratified columnar epithelium with dark cells (DC), light cells (Lc), and basal cells (asterisk) (F and G). A transition area between the posterior midgut (PMG) and the hindgut (Hg) (G). A pyloric valve (Pv) formed by a robust structure separates the two gut regions (H). Foregut composed of a constriction in the internal surface (arrows). Lu = lumen, N = nucleus, white arrow = nucleolus, Mf = muscle fibers, Bb = brush border, Am = amorphous material. Bars: 10 μm (A–D, F, and H) and 50 μm (E and G).

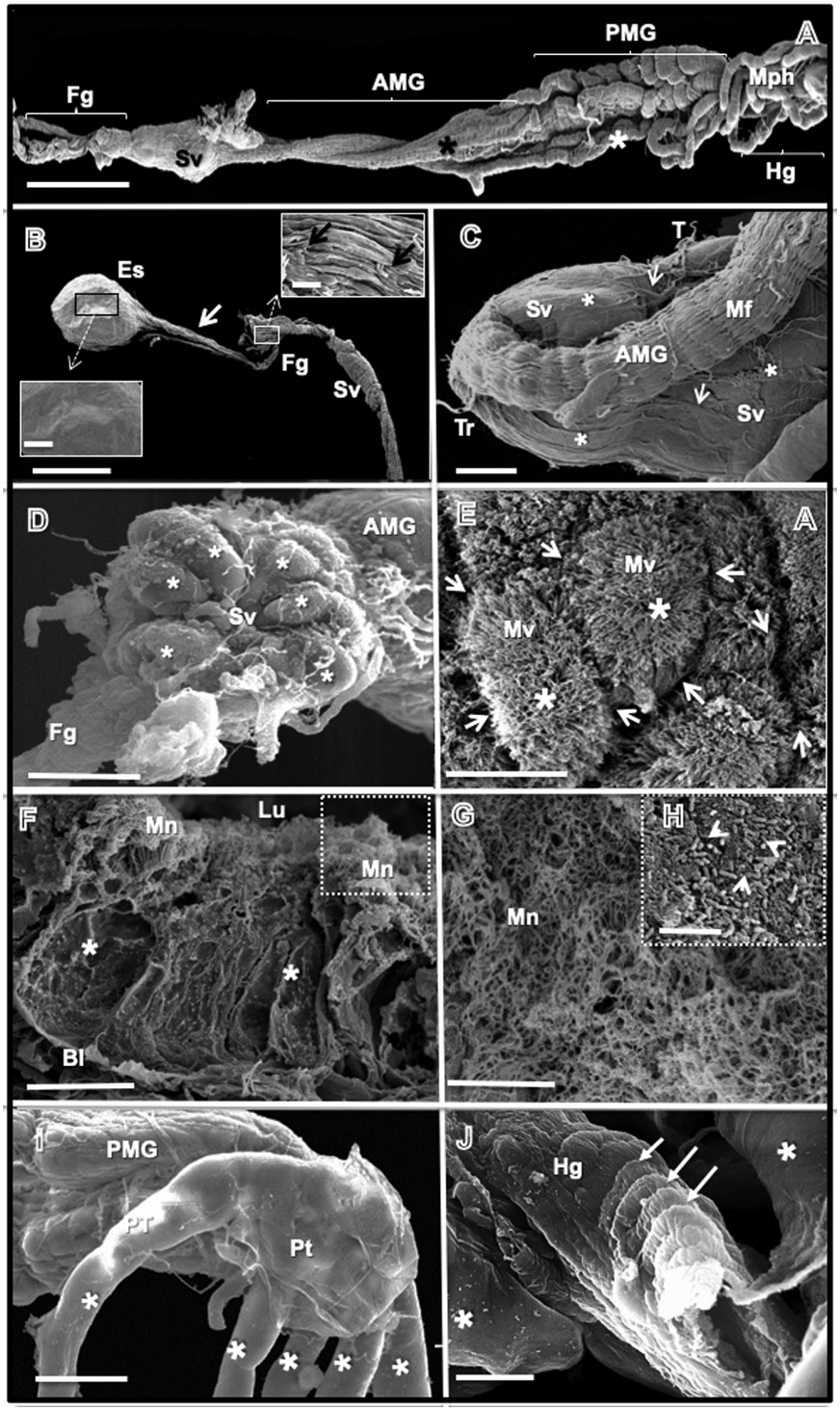

Fig. 2. Microanatomy (SEM) of the nonblood fed *Anopheles aquasalis* gut. (A) General view of a dissected mosquito gut. The main topographical divisions of the gut: foregut (Fg), anterior midgut (AMG), posterior midgut (PMG), and hindgut (Hg) are seen. The smooth surface (black asterisk) of the AMG is seen compared with the folded surface (white asterisk) of the PMG. The stomodeal valve (Sv) separates the foregut (Fg) from the AMG. Several collapsed Malpighi tubules (Mph) is attached in the hindgut (Hg). Bar: 5 μm. (B) Esophagus. The esophagus (Es) attached to the part of the foregut (Fg) by a small duct (arrow) through the stomodeal valve (Sv). Right and left insets = smooth surface of the esophagus (Es) and folded surface of the foregut (Fg) with constrictions (black arrow), respectively. Bars: 200 μm (B) and 100 μm (insets). (C) and (D) Stomodeal valve. The external surface of the stomodeal valve (Sv) shows the muscle network with longitudinal and circular fibers (white asterisks). Longitudinal fibers are quite visible with irregular distribution and some bifurcations (arrow). The surface of the AMG is covered by well-organized muscle fibers (Mf) and several trachea (Tr) that bifurcating to form smaller caliber tracheoles (T) (C). The internal surface of a stomodeal valve (Sv) shows six muscle protrusions (asterisks) (D). Fg = foregut, AMG = anterior midgut. Bars: 50 μm (C and D). (E) Surface of the epithelial digestive cells. SEM of the internal side of the AMG showing a large view of the cell surface of two epithelial digestive cells (asterisks) with well-delimited perimeter (arrows). Note the microvilli (Mv) covering their entire surfaces. Bar: 10 μm. (F) Fractured epithelial digestive cells. Columnar aspects of the epithelial digestive cells (asterisks) of the posterior midgut covered with straight microvilli (Mv) projecting to the lumen (Lu). A dense microfibrillar network (Mn) is seen

appears looser in the AMG because the basal lamina of several epithelial cells project among the muscle fibers (Fig. 5D and E). In the transition areas of the two midgut regions, small muscle fibers link the circular muscle fibers (Fig. 5E). A fractured area beneath the muscle network was observed by SEM, which showed the hexagonal shapes of the epithelial cells and part of their cytoskeleton (Fig. 5F).

The details of the cytoskeleton of the midgut muscle network were visualized by labeling actin filaments with the FITC-Phalloidin. The actin filaments intercalate in the two types of muscle fibers of the muscle network that covers the entire organ (Fig. 5H and I). The fluorescence images show that the muscle fibers are composed of sarcomeres organized in parallel matrices and helix structures (Fig. 5H). As seen by SEM, the muscle fibers are more compact in the AMG. Also, the sarcomeres appear more individualized in the circular muscle fibers (Fig. 5H and I). FITC-Phalloidin strongly labeled the stomodeal valve because it consists of densely distributed muscle fibers (Fig. 5G).

Sugar Residues of the Nonblood Fed *An. aquasalis* Midgut Labeled by Lectins

A set of FITC-labeled lectins was used to demonstrate by CLM the presence of specific terminal sugar residues in the *An. aquasalis* midgut. In the two midgut regions, the labeling patterns of the FITC-lectins are similar, but there are a few differences in the fluorescence intensities. When considering each of the FITC-lectins and their specific sugar-binding properties (Table 1), distinct fluorescence intensities are seen in the intracellular structures and the microvilli of the brush border of the epithelial cells in both the AMG and the PMG (Figs. 6 and 7).

TPNA, Con-A, and RCA labeled the microvilli that constitute the brush borders of the epithelial cells in both regions of the midgut (Figs. 6A–B, 6G–H, and 7G–H, respectively). LPL labeled the lateral membranes of the epithelial cells of the two areas but was stronger in the PMG (Fig. 6C and D). PNA labeled the lateral membranes, but only in the PMG, which is also exclusively labeled by UEA, but with lower intensity (Figs. 6A and B, and 7A and B). Interesting, only WGA labeled the basal lamina of the midgut epithelium and was stronger in the PMG (Fig. 6E and F). Finally, all the FITC-labeled lectins labeled vesicles and granules in the epithelial cytoplasm with no distinction between the two regions, except that WGA showed no clear labeling (Figs. 6 and 7). Con-A showed the strongest labeling of intracellular structures, and fluorescence intensity was similar in the two midgut regions (Fig. 6G and H).

Discussion

The main focus of this study was to understand the features of the nonblood-fed mosquito midgut of *An. aquasalis* females, a major vector of *P. vivax* (Haemosporida: Plasmodiidae) in the America continent. The midgut is the organ that stores the ingested bloodmeal and, consequently, is the first barrier that any vector-borne pathogen has to contend with in this mosquito vector. The use of a varied set of routine and modern morphological techniques allowed for a meticulous study that describes features of the midgut of the *An. aquasalis* females, including specific structures not yet described in New World *Anopheles* mosquito. The histology, SEM, and TEM showed the microanatomy and the ultrastructure of the organ. The cytochemical marker RR revealed some details of the ultrastructural aspects, and FITC-labeled lectins showed by CLM the presence of sugar residues.

The microanatomy of the dissected *An. aquasalis* gut revealed that the general anatomical structures are similar to other hematophagous mosquitoes and can be divided into three different regions: foregut, midgut, and hindgut (Richards 1975, Billingsley and Lehane 1996). However, this study also focused on the anatomical and ultrastructural details of midgut-associated structures such as the elaborate muscle network, the stomodeal valve, and the pyloric triangle. The nonblood-fed *An. aquasalis* midgut is an extensive and continuous microanatomical structure that begins with a tubular anterior AMG and a large distensible bag-shaped PMG with numerous folds, which guarantee an increase in space for the digestion and absorption of nutrients. The PMG is responsible for storage and digestion of the bloodmeal, which in general takes about 3–4 d (Billingsley 1990, Hecker 1997). These aspects contrast with nonhematophagous mosquitoes such as *Toxorhynchites theobaldi* (Diptera: Culicidae), where the midgut is divided into AMG1 (a short region with folds), AMG2 (an extended area without folds), and the PMG, which is the smallest part of the organ (Godoy et al. 2015).

The entire *An. aquasalis* midgut consists of a single layer of main columnar epithelial cells covered by thousands of microvilli projecting toward the lumen, which is similar to other mosquito midguts (Bertram and Bird 1961, Stäubli et al. 1966, Smith 1968, Hecker et al. 1971). This main microvillar columnar cell—also called digestive epithelial cells—are the basic units of the mosquito midgut (Richards 1975). The histology of the *An. aquasalis* midgut revealed that these main digestive epithelial cells have different TB stain affinities, which is similar to *Ae. aegypti* adults and larvae (Shahabuddin and Pimenta 1998, Fernandes et al. 2014). The TB stain is composed of a basic dye with metachromatic proprieties that has high affinity for acidic tissue components and stains nucleic acids blue and cytoplasmic polysaccharides\purple (Gokul and Skankar 2012). In *Ae. aegypti*, the light cells are less basophilic, lack microvilli, express high levels of vesicular ATPase, and are found at approximately the same frequency in the midgut. Different from *Ae. aegypti*, the *An. aquasalis* light and dark epithelial cells have similar amounts of microvilli on their surface. They also contain a very well-differentiated electron-dense cytoplasm. Although our study was not quantitative, the histological sections and TEM showed more dark cells than light cells in the *An. aquasalis* midgut. It is possible that in *An. aquasalis*, some light and dark cells constitute the same cellular type; however, the light cells may simply have suffered some damage or are in the process of differentiation. This is only conjecture, as no aspects of cellular division, apoptosis, or cell death were assayed in this study.

When considering the epithelial cell types present in the midgut, it qualitatively appeared that the light cells found in the *An. aquasalis* PMG had more organelles, such as well-developed endoplasmic reticulum and numerous vesicles and mitochondria. This suggests that these cells play a key role in the synthesis and secretion of proteolytic enzymes and the absorption of blood digestion products (Weaver and Scott 1990, Okuda et al. 2002). Usually,

in (C) covering the surfaces of fractured epithelial digestive cells (asterisks). Bl = basal lamina. Bar: 5 µm. (G) Microfibrillar network on the midgut epithelium. The presence of an intricate filamentous structure forming a dense microfibrillar network (Mn) is seen covering the posterior midgut epithelium. Bar: 5 µm. (H) Microbiota on the midgut epithelium. Numerous bacilliform bacteria (arrows) from the midgut microbiota are seen attached over the epithelium surface. Bar: 5 µm. (I) Pyloric triangle. Detail of the pyloric triangle (Pt) at the end of the PMG is showing a smooth surface and insertions of several Malpighi tubules (asterisks). Bar: 100 µm. (J) Hindgut. Details of hindgut (Hg) with delicate constrictions (arrow) in the external surface. Malpighi tubules (asterisks). Bar: 20 µm.

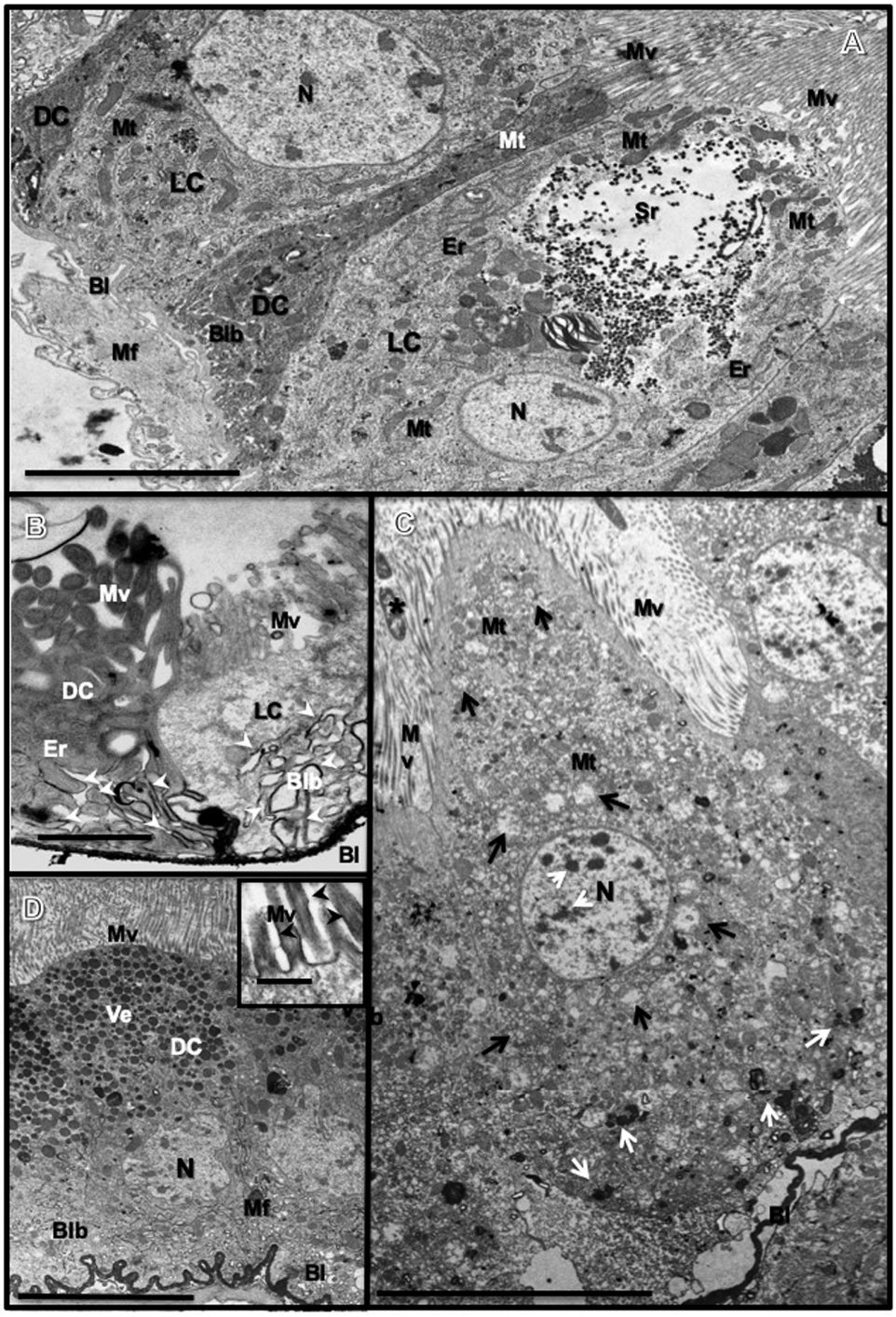

Fig. 3. Ultrastructure of the nonblood fed *Anopheles aquasalis* anterior midgut. (A) Epithelial cells of the anterior midgut. General view of composed images of two dark cells (DC) with two light cells (LC). The dark cells are slender with electron-dense cytoplasm showing fewer and distinct organelles contrasting with the light cells. Mv = microvilli, N = nucleus, Er = endoplasmic reticulum, Mt = mitochondria, Sr = storage reservoir with several granules, Blb = basal labyrinth, Bl = basal lamina, Mf = muscle fibers. Bar: 5 μm. (B) Epithelial cells of the anterior midgut RR labeling. Differences between light (LC) and cark cells (DC) evidenced by the RR labeling in the anterior midgut. Note the strong labeling (arrowheads) of the basal labyrinth (Blb) membranes. Mv = microvilli, Er = endoplasmic reticulum, Bl = basal lamina. Bar: 1 μm. (C) Epithelial cell of the posterior midgut. General view of an epithelial cell showing the surface with microvilli (Mv) and attached bacteria (asterisks). Several Mitochondria (Mt) are seen mainly in the apical cellular cytoplasm. A large rounded nucleus (N) with patched chromatin (white arrowheads) is located in the middle region of the cell. Vacuoles (black arrows) of different sizes are distributed in all cytoplasm regions. The basal cell cytoplasm has electron-dense granules (white arrows) with varied sizes. An electron-dense basal lamina (Bl) is seen in the basal region of the epithelial cell. Bar: 10 μm. (D) Dark Cell of the Posterior Midgut RR labeling. General view of the Dark Cell (DC) with numerous apical dense-labeled Vesicles (Ve). The inset image shows the organization of the dense electron material (arrowhead) on glicocalix of the microvilli (Mv). N = nucleus, Mf = muscular fibers, Mv = microvilli, Mt = mitochondria, Blb = basal labyrinth, Bl = basal lamina. Bars: 1 μm (C) and 10 μm (inset).

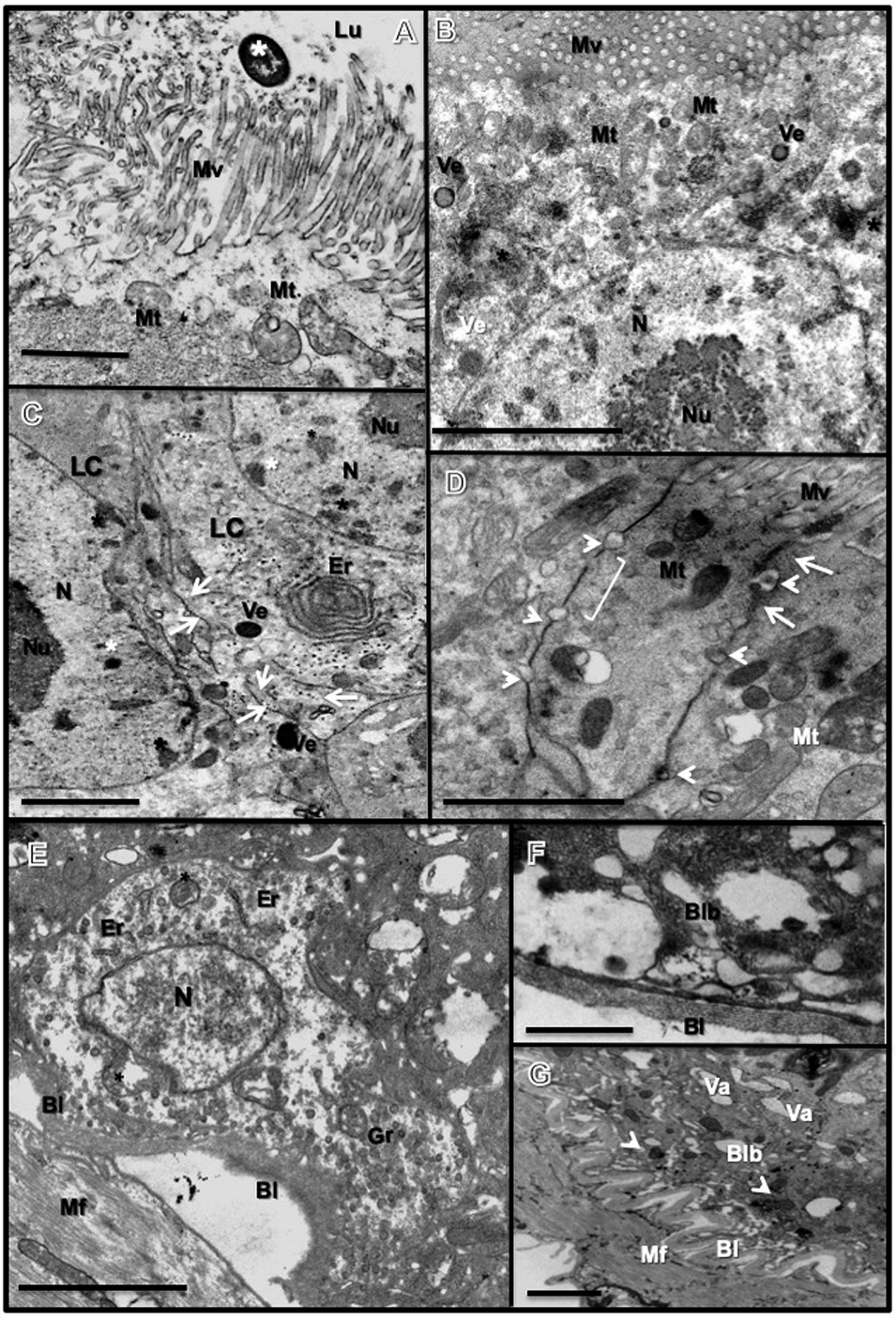

Fig. 4. Ultrastructure of the nonblood fed *Anopheles aquasalis*. (A) Cell surface of the epithelial cell. Large magnification of the surface of an epithelial cell showing details of the microvilli (Mv) projecting into the midgut lumen (Lu) and one attached bacteria (asterisk) on the posterior midgut (PMG). Mt = mitochondria. Bar: 2 μm. (B) Dark cell of the anterior midgut. Detailed aspects of the dark cell showing cytoplasm with mitochondria (Mt), rounded vesicles (Ve), and fine-dispersed granular material (white asterisks) between the mitochondria (Mt) and no visible endoplasmic reticulum. The nucleus (N) shows a nucleolus (Nu) with noncondensed chromatin. Bar: 5 μm. (C) Epithelial cell in the posterior midgut. Two light cells (LC) of the thoracic midgut showing cytoplasm with helicoidal endoplasmic reticulum (Er) and electron-dense vesicles (Ve), nuclei (N) exhibiting patched chromatins (white asterisks) and dense nucleolus (Nu) (C). Large magnification of the contact between epithelial cells showing adherent (arrows) and occlusion zones (white bracket) (D). Arrows = cell contact areas. Bars: 2 μm. (D) Cell junctions between epithelial cells. A Junctional Complex in the apical region of the cell showing joints of the adherent zone (arrowheads), occlusive zone (bracket) and Desmosomes (white arrow) (C). Mt = mitochondria. Mv = microvilli. Bar: 2 μm. (E) Basal epithelial cell. Small basal epithelial cell over the basal lamina (Bl) showing an electron-lucent cytoplasm with a large nucleus (N), Endoplasmic Reticulum (Er), numerous electron-dense Granules (Gr) and Mitochondria (asterisks). Mf = Muscle Fiber. Bar: 5 μm. (F) and (G) Basal region of the epithelial cell. Large magnification of basal region of Anterior Midgut showing the Basal Labyrinth (Blb) full of membrane invaginations and the basal lamina (Bl) composed of multiple parallel layers. Large magnification of the basal region of an epithelial cell in Posterior midgut showing an extensive basal labyrinth (Blb) supported by a folded basal lamina (Bl) and externally involved by muscle fibers (Mf) in the anterior midgut (G). Va = vacuoles. Arrowheads = electron-dense granules. Bars: 1 μm and 2 μm (G).

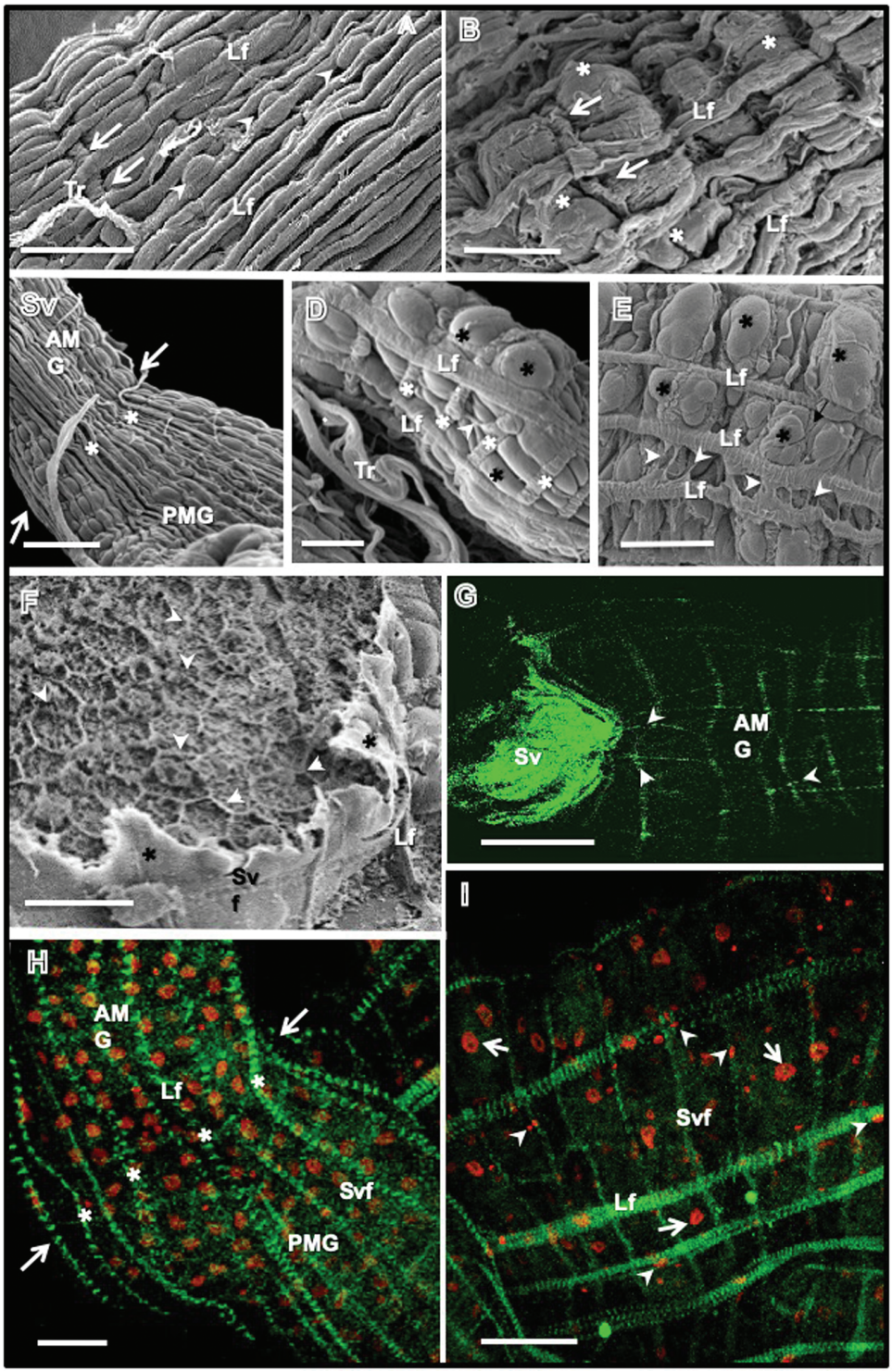

Fig. 5. External surface and the muscle network of *Anopheles aquasalis* midgut. (A) and (B) Anterior midgut. SEM general view of the external side of the anterior midgut showing an organized-tight muscle network comprised circular fibers (arrows) covered by longitudinal fibers (Lf). Projections of the muscle nuclei of the muscle fibers are seen (arrowheads) (A). Large magnification view of the muscle network showing basal projections of the epithelial cells (asterisks) among relaxed longitudinal fibers (Lf) and one circular fiber (arrow) (B). Tr = Tracheola. Bars: 20 μm (A) and 10 μm (B). (C) Transitional region between anterior and posterior midguts. Continuity of the muscle fibers (asterisks) between the two midgut regions (arrows) is seen. AMG = anterior midgut, PMG = posterior midgut. Bar: 50 μm. (D) and (E) Posterior midgut. General view of the external side of the posterior midgut showing details of the circular fibers (white asterisks) inserted beneath the longitudinal fibers (Lf) are shown (D). Small fibers (arrowheads) are linking two circular fibers (D) and longitudinal fibers (E). Black asterisks = epithelium projections. Tr = tracheola. Bars =20 μm. (F) Cytoskeleton of epithelial cells. Details of a fractured basal region of the Anterior Midgut showing the Cytoskeleton of the epithelial cells with hexagonal shape (arrows).Asterisks = broken Basal Lamina projections, Lf = Longitudinal Fiber, Cf = Circular Fiber. Bars: 10 μm. (G) Stomodeal valve (actin labeling by fluorescent Phalloidin), showing a massive concentration of filamentous actin filaments and linked (arrowheads) to the muscle network of the anterior midgut (AMG). Bar: 20 μm. (H) Transitional area between anterior and posterior midguts. The Phalloidin-stained muscle

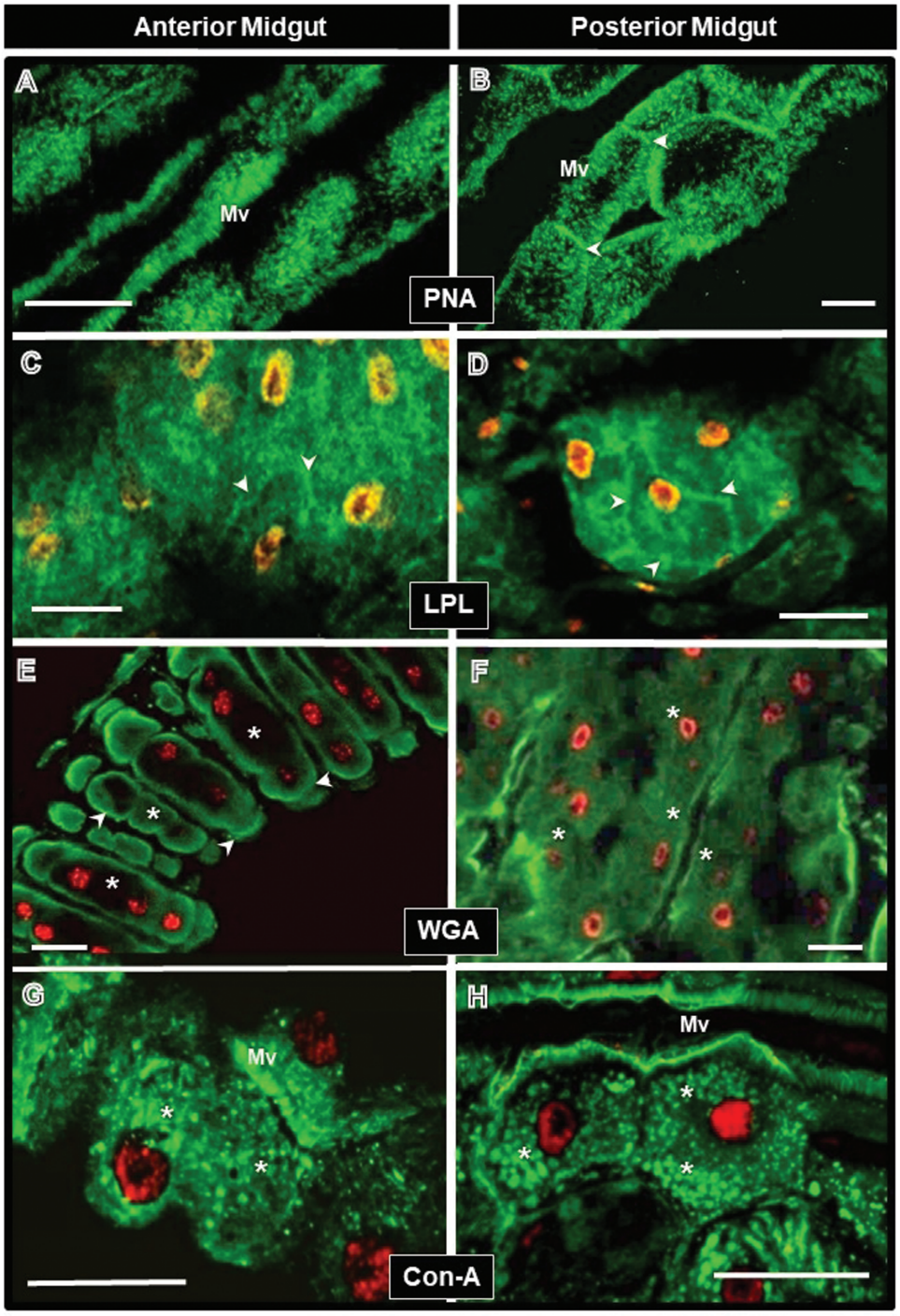

Fig. 6. Lectin labeling of the *Anopheles aquasalis* midgut. (A) and (B) WFA lectin with dispersed labeling of the cytoplasm of epithelial cells of the two midgut regions with stronger evidence in the anterior midgut (A). Absence of lectin labeling in muscle fiber locations of the two midgut regions (arrowheads). Nuclei = red color. Bars: 20 μm. (C) and (D) UEA lectin similarly labeled the two midgut regions evidencing the basal-lateral membrane (arrows). Occasional dissected Malpighi tubules (Mt) were strongly labeled by the lectin (D). Nuclei = red color. Bars: 20 μm. (E) and (F) BS1 lectin marked small vesicles (arrowheads) of the cytoplasm of the epithelial cells and the muscular fibers (Mf). Lu = midgut lumen. Nuclei = red color. Bars: 20 μm. (G) and (H) RCA lectin strongly labeled the microvilli (Mv) of the epithelial cells and basal-lateral membranes (arrowheads) of the two midgut regions. Bl = basal lamina, Lu = midgut lumen. Bars: 20 μm.

cytoplasmic secretory granules and vesicles are evident in the apical region of midgut cells of nonblood-fed mosquitoes and are immediately consumed after blood ingestion. It is considered that these structures contain precursors of the PM synthesis and initial

~~fibers (asterisks) are showing continuity between the two midgut regions (arrows). Details of the intercalated aspect of the actin filaments (green fluorescent la-~~beling) are seen in all muscle fibers. The rounded nuclei of the epithelial cells are distinctly labeled with red-fluorescence along the two midgut regions. Lf = longitudinal fiber, Cf = circular fiber. Bar: 50 μm. (I) Posterior midgut. Details of the Phalloidin-stained muscle fibers showing longitudinal (Lf) and circular fibers (Cf) composed by intercalated actin filaments. Note the presence of two types of red-fluorescent Nuclei, the rounded epithelial nuclei (arrows) and the small and fusiform nuclei of the muscle fibers (arrowheads). Bar: 20 μm.

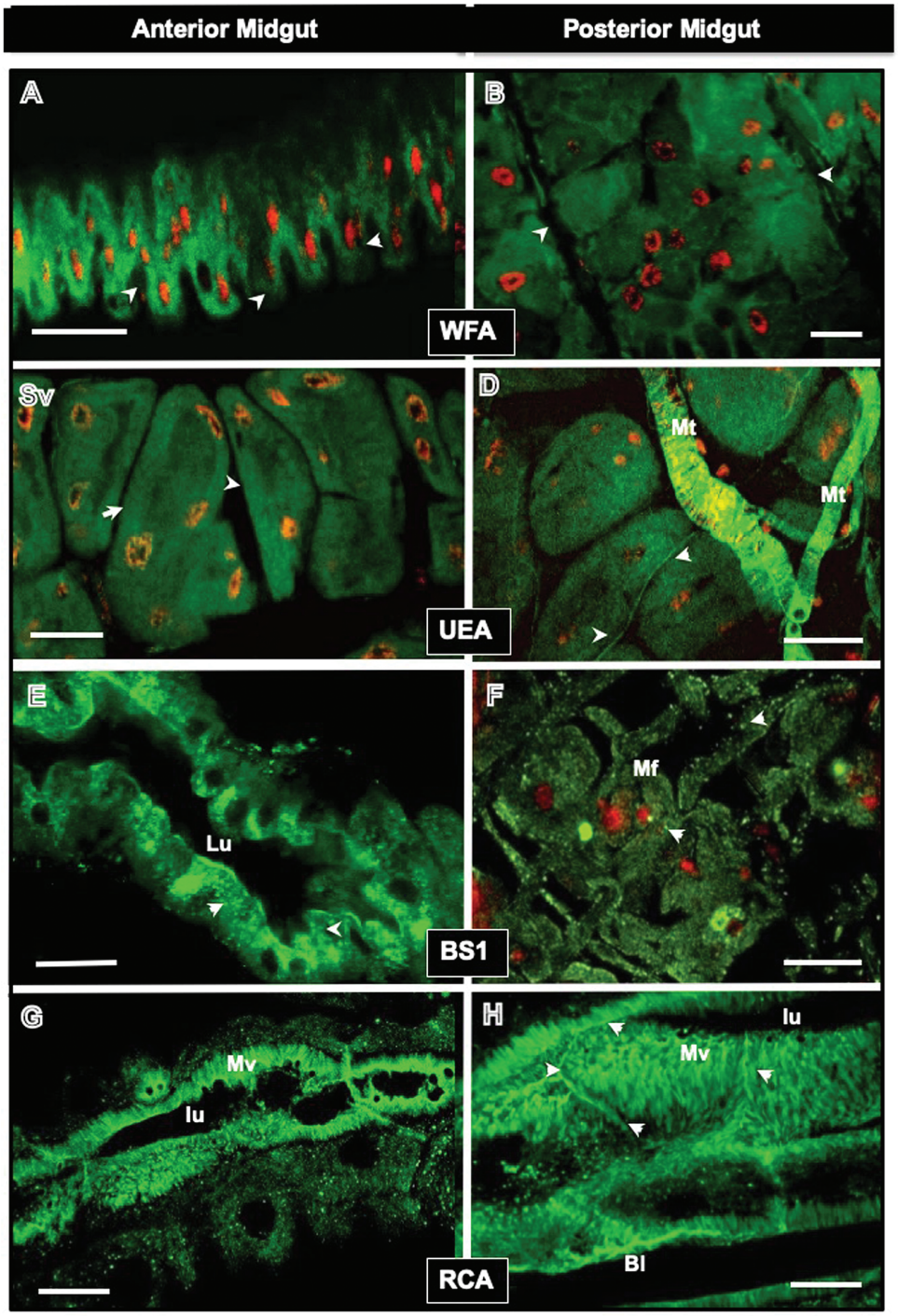

Fig. 7. Lectin labeling of the *Anopheles aquasalis* midgut. (A) and (B) WFA lectin with dispersed labeling of the cytoplasm of epithelial cells of the two midgut regions with stronger evidence in the thoracic midgut (A). Absence of lectin labeling in muscle fiber locations of the two midgut regions (arrowheads). Nuclei = red color. Bars: 20 µm. (C) and (D) UEA lectin similarly labeled the two midgut regions evidencing the basal-lateral membrane (arrows). Occasional dissected Malpighi tubules (Mt) were strongly labeled by the lectin (D). Nuclei = red color. Bars: 20 µm. (E) and (F) BS1 lectin marked small vesicles (arrowheads) of the cytoplasm of the epithelial cells and the muscular fibers (Mf). Lu = midgut lumen. Nuclei = red color. Bars: 20 µm. (G) and (H) RCA lectin strongly labeled the microvilli (Mv) of the epithelial cells and basal-lateral membranes (arrowheads) of the two midgut regions. Bl = basal lamina, Lu = midgut lumen. Bars: 20 µm.

enzyme products for blood digestion (Okuda et al. 2002, 2005; Devenport et al. 2004; Cázares-Raga et al. 2014). Future comparative kinetic studies of nonblood-fed midguts and midguts at distinct times after the ingestion of the bloodmeal are necessary to better characterize the role that midgut epithelial cells play in blood digestion and the synthesis of the PM.

The RR labeling of the midgut epithelium accentuated differences between the epithelial cells of the *An. aquasalis* midgut, which included stronger labeling of the surface and the cytoplasm of the dark cells. There is no similar study showing such details of the midgut cells of other *Anopheles* mosquitoes. The RR labeling defined the presence of polyanionic glycosaminoglycans (GAG) and anionic

polysaccharides in the cell surface. The GAG is a sulfated glycosaminoglycan composed of chains of alternating sugars (N-acetylgalactosamine and glucuronic acid), which are considered midgut surface ligands for *Plasmodium* sp. invasion (Sinnis et al. 2007, Dinglasan et al. 2007). Therefore, it should be considerate that dark epithelial cells express more GAGs and are those preferentially involved with *Plasmodium* invasion. More in-depth studies focusing on these midgut cells are needed to ascertain their physiology and their possible importance in *Plasmodium* invasion.

The presence of a microvilli-associated network (MN) in the *An. aquasalis* midgut epithelium is structurally similar to what has been observed in *Ae. aegypti* and *Culex quinquefasciatus* (Diptera: Culicidae). This MN consists of widespread fine membranous strands located between the midgut lumen and the microvillar layer (Zieler et al. 1998, 2000, Okuda et al. 2002). The role of the MN over the midgut epithelium is still unclear. It has been suggested that it prevents direct contact between the intestinal epithelium and the bloodmeal, that it prevents attack between ingested phagocytes and mosquito cells, or that it hinders the contact between parasites and arboviruses and midgut cells (Zieler et al. 1998, 2000). Interestingly, we observed that bacilliform bacteria and filamentous material attach to the MN. Because the observations are from nonblood-fed mosquitoes, these bacteria are probably components of the natural microbiota that exists in the midgut of several insects including those found by metagenomic studies in *An. aquasalis*, as previously described by our group (Villegas and Pimenta 2014). As suggested in previous studies, such bacteria are probably acquired from the environment (review in Stoffolano and Haselton 2013).

In this study, SEM and CLM revealed features of the topography and the cytoskeleton of the complex muscle network located on the external midgut surface of nonblood-fed *An. aquasalis*. The midgut muscle network is composed of multifaceted and well-arranged layers of circular and longitudinal fibers that cover and surround the entire organ. A previous comparative study of non-blood-fed and *P. vivax* blood-fed *An. aquasalis* (Baia-da-Silva et al. 2018) using SEM and TEM observed similar aspects of the midgut muscle network at distinct intervals after blood ingestion. However, actin labeling confirmed details of the cytoskeleton of this muscle network; it is composed of filaments with an intercalated aspect noted in the two types of the muscle fibers. These structures contain well-defined sarcomeres, and the muscle fibers appear continuous between the AMG and PMG. Indeed, this complex muscle network maintains the integrity of the midgut epithelium. After blood ingestion, the midgut epithelial cells become flattened, and it takes 72 h to returns to its initial shape after the complete blood digestion (Dana et al. 2005, Sodja et al. 2007).

FITC-lectin labeling is one of the best tools for localizing surface carbohydrates and sugar ligands on cell surfaces. Sugar residues on the surface of host cells are related to cellular phagocytosis and the binding and invasion of pathogens (Sharon et al. 1981, Roy and Mandal 2016, Szymanski et al. 2017). A set of fluorescent lectins was previously used in the *Ae. aegypti* midgut (Zieler et al. 2000). In this study, the same set of eight FITC lectins was used to label the *An. aquasalis* midgut. We observed different fluorescence intensities in different regions of the epithelial cells of the midgut, which demonstrates the diversity of sugar residues present. For example, we observed strong labeling of Con-A, WGA, and Lentil lectins and intermediate labeling of UEA—which is similar to what has been described in the *Ae. aegypti* midgut—but RCA and PNA labeling was distinct and more evident in *An. aquasalis* (Zieler et al. 2000).

Our FITC-lectin data suggest that the *An. aquasalis* midgut epithelium comprises mainly of α-D-mannosyl α-D-glucosyl carbohydrates, fucolyzed regions of the bi- and triantennary complexes of the N-glycan type, N-acetylgalactosamine, β-d-galactose, and Core 1 O-glycan Galβ1-3GalNAcα1-Ser/Thr (T antigen). Moreover, that the microvilli layer of the *An. aquasalis* midgut stains strongly with PNA, CONA, RCA, and LENTIL indicates that the microvilli layer contains several types of sugar residues. Glycoconjugates of the microvilli in the midgut epithelium of vectors are targeted specifically by *Plasmodium* and other pathogens, such as galectin, O-linked glycans, GAGS (Pimenta et al. 1992, Welburn et al. 1994, Kroschewski et al. 2003, Kamhawi et al. 2004, Dinglasan et al. 2005).

However, LPL, WGA, CONA, WFA, UEA, RCA, and LENTIL labeled the baso-lateral region of the *An. aquasalis* midgut epithelium, which indicates the existence of distinct types of sugar residues on the surface. Rudin and Hecker (1989) observed intense marking of the basolateral membranes of the *Anopheles stephensi* (Diptera: Culicidae) and *Ae. aegypti* midguts with Con-A, but weak WGA binding. Distinctly, we found that WGA was highly specific for the baso-lateral membranes of the *An. aquasalis* midgut. FITC-lectin labeling of the baso-lateral region of the *An. aquasalis* midgut epithelium detected the following sugar residues: α-D-Galactosyl, N-acetyl-α-D-glacactosamine, N-acetyl-D-galactosamine, N-acetyl-α-D-galactosamine, N-acetyl-neurominic acid, GlcNAcβ1-4GlcNAcβ1-4GlcNAc, Neu5Ac (sialic acid), Fucα1-2Gal-R and galNaC, α-D-mannosyl α-D-glucosyl, fucolyzed regions of the bi- and triantennary complexes of the N-glycan type, N-acetylgalactosamine, β-D-galactose and Core 1 O-glycan Galβ1-3GalNAcα1-Ser/Thr (T antigen). Probably, some of these sugar residues are present in the basal lamina of the midgut and are the targets and ligands for the recognition, access, and binding of *Plasmodium* oocysts. Inside the midgut of their specific mosquito vector, the *Plasmodium* ookinetes can recognize ligands, attach, invade, and cross the epithelial cells (Zieler et al. 2000, Dinglasan and Jacobs-Lorena 2005). Further studies of the sugar composition of the *Anopheles* midgut are of fundamental importance to understand the interaction between vectors and distinct *Plasmodium* species.

Conclusion

In conclusion, the use of diverse morphological methods, such as traditional and modern techniques, revealed details of the microanatomy of the *An. aquasalis* midgut and features of several associated organs. These data will undoubtedly support future studies on the interaction between *Plasmodium* spp. (Haemosporida: Plasmodiidae) and this life-threatening American mosquito vector.

Acknowledgments

This study was partially funded by the Bill and Melinda Gates Foundation (TransEpiStudy), by the National Institutes of Health grant R01AI031478, and by the following Brazilian agencies: Foundation of the Institute Oswaldo Cruz (FIOCRUZ); Brazilian Council for Scientific and Technological Development (CNPq/MCTI/CAPES/SCTIE/MS); Coordination of Improvement of Higher Level Personnel (CAPES/MEC); Strategic Programme for Supporting Health Research (PAPES V); Science Without Borders Programme - CNPq-CAPES; National Institutes of Science and Technology – INCT Elimina and INCT Molecular Entomology; Minas Gerais State Research Support Foundation (FAPEMIG); Supporting Programme for Young Ph.D. Professors – Federal University of Bahia (PROPESQ/UFBA); and Amazonas State Research Support (FAPEAM). M.V.G.L., N.F.C.S., P.F.P.P., and W.M.M. are senior research fellows supported by CNPq.

References Cited

Bahia, A. C., M. S. Kubota, A. J. Tempone, W. D. Pinheiro, W. P. Tadei, N. F. Secundino, Y. M. Traub-Csekö, and P. F. Pimenta. 2010. *Anopheles aquasalis* infected by *Plasmodium vivax* displays unique gene expression profiles when compared to other malaria vectors and plasmodia. PLoS One 5: e9795.

Bahia, A. C., M. S. Kubota, A. J. Tempone, H. R. Araújo, B. A. Guedes, A. S. Orfanó, W. P. Tadei, C. M. Ríos-Velásquez, Y. S. Han, N. F. Secundino, et al. 2011. The JAK-STAT pathway controls *Plasmodium vivax* load in early stages of *Anopheles aquasalis* infection. Plos Negl. Trop. Dis. 5: e1317.

Bahia, A. C., J. H. Oliveira, M. S. Kubota, H. R. Araújo, J. B. Lima, C. M. Ríos-Velásquez, M. V. Lacerda, P. L. Oliveira, Y. M. Traub-Csekö, and P. F. Pimenta. 2013. The role of reactive oxygen species in *Anopheles aquasalis* response to *Plasmodium vivax* infection. PLoS One 8: e57014.

Baia-da-Silva, D. C., L. C. S. Alvarez, O. V. Lizcano, F. T. M. Costa, S. C. P. Lopes, A. S. Orfanó, D. O. Pascoal, R. Nacif-Pimenta, et al. 2018. The role of the peritrophic matrix and red blood cell concentration in *Plasmodium vivax* infection of *Anopheles aquasalis*. Parasit Vectors 11: 148.

Baia-da-Silva, D. C., A. S. Orfanó, R. Nacif-Pimenta, F. F. de Melo, S. Simões, I. Cabral, M. V. G. Lacerda, M. D. G. B. Guerra, W. M. Monteiro, N. F. C. Secundino, and P. F. P. Pimenta, 2019. The Midgut Muscle Network of *Anopheles aquasalis* response to *Plasmodium vivax* infection. (Culicidae, Anophelinae): Microanatomy and Structural Modification After Blood Meal and *Plasmodium vivax* (Haemosporida, Plasmodiidae) Infection. J Med Entomol 56: 421–431.

Bauer, P., W. Rudin, and H. Hecker. 1977. Ultrastructural changes in midgut cells of female *Aedes aegypti* L. (Insecta, Diptera) after starvation or sugar diet. Cell Tissue Res. 177: 215–219.

Bennink, S., M. J. Kiesow, and G. Pradel. 2016. The development of malaria parasites in the mosquito midgut. Cell Microbiol. 18: 905–918.

Bertram, D. S., and R. G. Bird. 1961. Studies on mosquito-borne viruses in their vector. I. The normal fine structure of the midgut epithelium of adult female *Aedes aegypti* L. and the functional significance of its modifications following a blood meal. Trans R Soe Trop Med Hyg. 54: 362–365

Billingsley, P. F. 1990. The midgut ultrastructure of hematophagous insects. Annu. Rev. Entomol. 35:219–248.

Billingsley, P. F., and M. J. Lehane. 1996. Structure and ultrastructure of the insect midgut. *In* M. J. Lehane and P. F. Billingsley (eds.), Biology of the insect midgut. Springer, Dordrecht, The Netherlands.

Brown, M. R., J. W. Crim, and A. O. Lea. 1986. FMRFamide- and pancreatic polypeptide-like immunoreactivity of endocrine cells in the midgut of a mosquito. Tissue Cell 18: 419–428.

Cázares-Raga, F. E., B. Chávez-Munguía, C. González-Calixto, A. P. Ochoa-Franco, M. A. Gawinowicz, M. H. Rodríguez, and F. C. Hernández-Hernández. 2014. Morphological and proteomic characterization of midgut of the malaria vector *Anopheles albimanus* at early time after a blood feeding. J. Proteomics 111: 100–112.

Chapman, R. F. 1998. The insects: structure and function. Cambridge University Press, Harvard, United Kingdom.

Conn, J., A. F. Cockburn, and S. E. Mitchell. 1993. Population differentiation of the malaria vector *Anopheles aquasalis* using mitochondrial DNA. J. Hered. 84: 248–253.

Dana, A. N., Y. S. Hong, M. K. Kern, M. E. Hillenmeyer, B. W. Harker, N. F. Lobo, J. R. Hogan, P. Romans, and F. H. Collins. 2005. Gene expression patterns associated with blood-feeding in the malaria mosquito *Anopheles gambiae*. BMC Genomics 6: 5.

Da Silva, A. N., C. C. Dos Santos, R. N. Lacerda, E. P. Santa Rosa, R. T. De Souza, D. Galiza, I. Sucupira, J. E. Conn, and M. M. Póvoa. 2006. Laboratory colonization of *Anopheles aquasalis* (Diptera: Culicidae) in Belém, Pará, Brazil. J. Med. Entomol. 43: 107–109.

Deane, L. M. 1986. Malaria vectors in Brazil. Mem. Inst. Oswaldo Cruz, 81 (suppl.3): 5–14.

Devenport, M., H. Fujioka, and M. Jacobs-Lorena. 2004. Storage and secretion of the peritrophic matrix protein Ag-Aper1 and trypsin in the midgut of *Anopheles gambiae*. Insect Mol. Biol. 13: 349–358.

Dierichs, R. 1979. Ruthenium red as a stain for electron microscopy. Some new aspects of its application and mode of action. Histochemistry 64: 171–187.

Dinglasan, R. R., and M. Jacobs-Lorena. 2005. Insight into a conserved lifestyle: protein-carbohydrate adhesion strategies of vector-borne pathogens. Infect. Immun. 73: 7797–7807.

Dinglasan, R. R., J. M. Porter-Kelley, U. Alam, and A. F. Azad. 2005. Peptide mimics as surrogate immunogens of mosquito midgut carbohydrate malaria transmission blocking targets. Vaccine 23: 2717–2724.

Dinglasan, R. R., A. Alaganan, A. K. Ghosh, A. Saito, T. H. van Kuppevelt, and M. Jacobs-Lorena. 2007. *Plasmodium falciparum* ookinetes require mosquito midgut chondroitin sulfate proteoglycans for cell invasion. Proc. Natl. Acad. Sci. USA 104: 15882–15887.

Fairley, T. L., C. W. Kilpatrick, and J. E. Conn. 2005. Intragenomic heterogeneity of internal transcribed spacer rDNA in neotropical malaria vector *Anopheles aquasalis* (Diptera: Culicidae). J. Med. Entomol. 42: 795–800.

Fernandes, K. M., C. A. Neves, J. E. Serrão, and G. F. Martins. 2014. *Aedes aegypti* midgut remodeling during metamorphosis. Parasitol. Int. 63: 506–512.

Flores-Mendoza, C., R. A. Cunha, D. S. Rocha, and R. Lourenço-de-Oliveira. 1996. Identification of food sources of *Anopheles aquasalis* (Diptera: Culicidae) by precipitin test in the State of Rio de Janeiro, Brazil. Rev. Saude Publ. 30: 129–134.

Godoy, R. S., K. M. Fernandes, and G. F. Martins. 2015. Midgut of the non-hematophagous mosquito *Toxorhynchites theobaldi* (Diptera, Culicidae). Sci. Rep. 5: 15836.

Hay, S. I., M. E. Sinka, R. M. Okara, C. W. Kabaria, P. M. Mbithi, C. C. Tago, D. Benz, P. W. Gething, R. E. Howes, A. P. Patil, et al. 2010. Developing global maps of the dominant *Anopheles* vectors of human malaria. PLoS Med. 7: e1000209.

Hecker, H. 1977. Structure and function of midgut epithelial cells in Culicidae mosquitoes (Insecta, Diptera). Cell Tissue Res. 184: 321–341.

Hecker, H., T. A. Freyvogel, H. Briegel, and R. Steiger. 1971. The ultrastructure of midgut epithelium in *Aedes aegypti* (L). (Insecta, Diptera) males. Acta Trop. 28: 275–290.

Houk, E. J. 1977. Midgut ultrastructure of *Culex tarsalis* (Diptera: Culicidae) before and after a bloodmeal. Tissue Cell 9: 103–118.

Houk, E. J., and J. L. Hardy. 1982. Midgut cellular responses to blood meal digestion in the mosquito, *Culex tarsalis* Coquillett (Diptera: Culicidae). Int. J. Insect Morphol. Embryol. 11: 109–119.

Kamhawi, S., M. Ramalho-Ortigao, V. M. Pham, S. Kumar, P. G. Lawyer, S. J. Turco, C. Barillas-Mury, D. L. Sacks, and J. G. Valenzuela. 2004. A role for insect galectins in parasite survival. Cell 119: 329–341.

Kroschewski, H., S. L. Allison, F. X. Heinz, and C. W. Mandl. 2003. Role of heparan sulfate for attachment and entry of tick-borne encephalitis virus. Virology 308: 92–100.

Laubach, H. E., L. Validum, J. A. Bonilla, A. Agar, R. Cummings, C. Mitchell, R. R. Cuadrado, and C. J. Palmer. 2001. Identification of *Anopheles aquasalis* as a possible vector of malaria in Guyana, South America. West Indian Med. J. 50: 319–321.

Maldonado, V., H. J. Finol, and J. C. Navarro. 1997. *Anopheles aquasalis* eggs from two Venezuelan localities compared by scanning electron microscopy. Mem. Inst. Oswaldo Cruz. 92: 487–491.

Martins-Campos, K. M., A. Kuehn, A. Almeida, A. P. M. Duarte, V. S. Sampaio, Í. C. Rodriguez, S. G. M. da Silva, C. M. Ríos-Velásquez, J. B. P. Lima, P. F. P. Pimenta, et al. 2018. Infection of *Anopheles aquasalis* from symptomatic and asymptomatic *Plasmodium vivax* infections in Manaus, western Brazilian Amazon. Parasit. Vectors 11: 288.

Menghi, G., L. Marchetti, A. M. Bondi, and G. Materazzi. 1997. Contribution of confocal laser scanning microscopy to glycochemistry of mouse and rat submandibular glands by single and double lectin staining. Eur. J. Histochem. 41: 91–104.

Okuda, K., A. de Souza Caroci, P. E. Ribolla, A. G. de Bianchi, and A. T. Bijovsky. 2002. Functional morphology of adult female *Culex quinquefasciatus* midgut during blood digestion. Tissue Cell 34: 210–219.

Okuda, K., A. Caroci, P. Ribolla, O. Marinotti, A. G. de Bianchi, and A. T. Bijovsky. 2005. Morphological and enzymatic analysis of the

midgut of *Anopheles darlingi* during blood digestion. J. Insect Physiol. 51: 769–776.

Onken, H., and D. F. Moffett. 2015. Fluid absorption in the isolated midgut of adult female yellow fever mosquitoes (*Aedes aegypti*). J. Exp. Biol. 218: 2023–2029.

Orfanó, A. S., A. P. Duarte, A. Molina-Cruz, P. F. Pimenta, and C. Barillas-Mury. 2016a. *Plasmodium yoelii nigeriensis* (N67) is a robust animal model to study malaria transmission by South American anopheline mosquitoes. PLoS One 11: e0167178.

Orfanó, A. S., R. Nacif-Pimenta, A. P. Duarte, L. M. Villegas, N. B. Rodrigues, L. C. Pinto, K. M. Campos, Y. T. Pinilla, B. Chaves, M. G. Barbosa Guerra, et al. 2016b. Species-specific escape of *Plasmodium* sporozoites from oocysts of avian, rodent, and human malarial parasites. Malar. J. 15: 394.

Perez, A. M., and J. Conn. 1992. A polytene chromosome study of four populations of *Anopheles aquasalis* from Venezuela. Genome 35: 327–331.

Pimenta, P. F., and W. de Souza. 1983. *Leishmania mexicana amazonensis*: surface charge of amastigote and promastigote forms. Exp. Parasitol. 56: 194–206.

Pimenta, P. F., M. Touray, and L. Miller. 1994. The journey of malaria sporozoites in the mosquito salivary gland. J. Eukaryot. Microbiol. 41: 608–624.

Pimenta, P. F., S. J. Turco, M. J. McConville, P. G. Lawyer, P. V. Perkins, and D. L. Sacks. 1992. Stage-specific adhesion of *Leishmania promastigotes* to the sandfly midgut. Science 256: 1812–1815.

Pimenta, P. F., A. S. Orfano, A. C. Bahia, A. P. Duarte, C. M. Ríos-Velásquez, F. F. Melo, F. A. Pessoa, G. A. Oliveira, K. M. Campos, L. M. Villegas, et al. 2015. An overview of malaria transmission from the perspective of Amazon *Anopheles* vectors. Mem. Inst. Oswaldo Cruz. 110: 23–47.

Pinilla, Y. T., S. C. P. Lopes, V. S Sampaio, F. S. Andrade, G. C. Melo, A. S. Orfanó, N. F. C. Secundino, M. G. V. B. Guerra, M. V. G. Lacerda, K. C. Kobylinski, et al. 2018. Promising approach to reducing Malaria transmission by ivermectin: Sporontocidal effect against *Plasmodium vivax* in the South American vectors *Anopheles aquasalis* and *Anopheles darlingi*. PLoS Negl. Trop. Dis. 12: e0006221.

Richards, A. G. 1975. The ultrastructure of the midgut of hematophagous insects. Acta Trop. 32: 83–95.

Rios-Velásquez, C. M., K. M. Martins-Campos, R. C. Simões, T. Izzo, E. V. dos Santos, F. A. Pessoa, J. B. Lima, W. M. Monteiro, N. F. Secundino, M. V. Lacerda, et al. 2013. Experimental *Plasmodium vivax* infection of key *Anopheles* species from the Brazilian Amazon. Malar. J. 12: 460.

Roy, S., and C. Mandal. 2016. *Leishmania donovani* utilize sialic acids for binding and phagocytosis in the macrophages through selective utilization of siglecs and impair the innate immune arm. PLoS Negl. Trop. Dis. 10: e0004904.

Rudin, W., and H. Hecker. 1989. Lectin-binding sites in the midgut of the mosquitoes *Anopheles stephensi* Liston and *Aedes aegypti* L. (Diptera: Culicidae). Parasitol. Res. 75: 268–279.

Secundino, N. F., I. Eger-Mangrich, E. M. Braga, M. M. Santoro, and P. F. Pimenta. 2005. *Lutzomyia longipalpis* peritrophic matrix: formation, structure, and chemical composition. J. Med. Entomol. 42: 928–938.

Shahabuddin, M., and P. F. Pimenta. 1998. *Plasmodium gallinaceum* preferentially invades vesicular ATPase-expressing cells in *Aedes aegypti* midgut. Proc. Natl. Acad. Sci. USA 95: 3385–3389.

Sharon, N., Y. Eshdat, F. J. Silverblatt, and I. Ofek. 1981. Bacterial adherence to cell surface sugars. Ciba Found. Symp. 80: 119–141.

Sinka, M. E., M. J. Bangs, S. Manguin, Y. Rubio-Palis, T. Chareonviriyaphap, M. Coetzee, C. M. Mbogo, J. Hemingway, A. P. Patil, W. H. Temperley, et al. 2012. A global map of dominant malaria vectors. Parasit. Vectors 5: 69.

Sinnis, P., A. Coppi, T. Toida, H. Toyoda, A. Kinoshita-Toyoda, J. Xie, M. M. Kemp, and R. J. Linhardt. 2007. Mosquito heparan sulfate and its potential role in malaria infection and transmission. J. Biol. Chem. 282: 25376–25384.

Smith, D. S. 1968. Insect cells: their structure and functions, pp. 223–266. Oliver and Boyd Press, Edinburgh, United Kingdom.

Sodja, A., H. Fujioka, F. J. Lemos, M. Donnelly-Doman, and M. Jacobs-Lorena. 2007. Induction of actin gene expression in the mosquito midgut by blood ingestion correlates with striking changes of cell shape. J. Insect Physiol. 53: 833–839.

Sridharan, G., and A. A. Shankar. 2012. Toluidine blue: a review of its chemistry and clinical utility. J. Oral Maxillofac. Pathol. 16: 251–255.

Stäubli, W., T. A. Freyvogel, and J. Suter. 1966. Structural modification of the endoplasmic reticulum of the midgut epithelial cells of mosquitoes in relation to blood intake. J Microsc. 5: 189–204.

Stoffolano, J. G., Jr., and A. T. Haselton. 2013. The adult Dipteran crop: a unique and overlooked organ. Annu. Rev. Entomol. 58: 205–225.

Szymanski, C. M., R. L. Schnaar, and M. Aebi. 2017. Bacterial and viral infections. *In* A. Varki, R. D. Cummings, J. D. Esko, et al., (eds.), Essentials of glycobiology [Internet], 3rd ed. Cold Spring Harbor Laboratory Press, Cold Spring Harbor, NY.

Villegas, L. M., and P. F. Pimenta. 2014. Metagenomics, paratransgenesis and the *Anopheles* microbiome: a portrait of the geographical distribution of the anopheline microbiota based on a meta-analysis of reported taxa. Mem. Inst. Oswaldo Cruz. 109: 672–684.

Weaver, S. C., and T. W. Scott. 1990. Ultrastructural changes in the abdominal midgut of the mosquito, *Culiseta melanura*, during the gonotrophic cycle. Tissue Cell 22: 895–909.

Welburn, S. C., I. Maudlin, and D. H. Molyneux. 1994. Midgut lectin activity and sugar specificity in teneral and fed tsetse. Med. Vet. Entomol. 8: 81–87.

WHO. 2018. World malaria report 2018. World Health Organization, Geneva, Switzerland.

Zieler, H., C. F. Garon, E. R. Fischer, and M. Shahabuddin. 1998. Adhesion of *Plasmodium gallinaceum* ookinetes to the *Aedes aegypti* midgut: sites of parasite attachment and morphological changes in the ookinete. J. Eukaryot. Microbiol. 45: 512–520.

Zieler, H., C. F. Garon, E. R. Fischer, and M. Shahabuddin. 2000. A tubular network associated with the brush-border surface of the *Aedes aegypti* midgut: implications for pathogen transmission by mosquitoes. J. Exp. Biol. 203: 1599–1611.